Published in final edited form as:
Sci Signal. ; 2(98): ra77. doi:10.1126/scisignal.2000466.

Ca^{2+} puffs originate from pre-established stable clusters of inositol trisphosphate receptors

Ian F. Smith[1], **Steven M. Wiltgen**[1], **Jianwei Shuai**[3], and **Ian Parker**[1,2]

[1]Department of Neurobiology and Behavior, University of California, Irvine CA 92697-4550

[2]Department of Physiology & Biophysics, University of California, Irvine CA 92697-4550

[3]Department of Physics, Xiamen University, Xiamen, China

Abstract

Intracellular Ca^{2+} signaling crucially depends upon the clustered organization of inositol trisphosphate receptors (IP_3Rs) in the ER membrane that liberate Ca^{2+} to generate local signals known as Ca^{2+} puffs. Clusters of IP_3Rs have been proposed to assemble rapidly in response to IP_3 itself. We tested this hypothesis by using flash photolysis of caged IP_3 in conjunction with high resolution Ca^{2+} imaging to monitor the activity and localization of individual IP_3Rs within intact mammalian cells. Our results indicate that puffs arising with latencies as short as 100–200 ms following photorelease of IP_3 already involve several ($n \geq 4$) IP_3R channels, and that this number does not subsequently grow. Moreover, single active IP_3Rs show very limited motility, and stochastic simulations suggest that aggregation of IP_3Rs at puff sites by a diffusional trapping mechanism would require many seconds. We thus find no evidence for rapid, IP_3-regulated clustering of IP_3Rs in intact cells, but instead conclude that puff sites represent pre-established, stable clusters of IP_3Rs and that functional IP_3Rs are not readily diffusible within the ER membrane.

Keywords

calcium signaling; TIRF microscopy; ion-channel; optical patch-clamp; inositol trisphosphate receptor; spatial organization; clustering

INTRODUCTION

Inositol trisphosphate receptors (IP_3Rs) are Ca^{2+}-permeable channels in the membrane of the endoplasmic reticulum (ER) that liberate Ca^{2+} sequestered in ER stores to generate cytosolic Ca^{2+} signals that control ubiquitous and diverse cellular functions including gene expression, secretion and synaptic plasticity (1). Opening of the IP_3R channel is regulated by the soluble second messenger IP_3, produced in response to activation of numerous G-protein and tyrosine kinase-linked cell surface receptors (2). However, channel gating also requires cytosolic Ca^{2+} itself (2,3), creating a positive feedback mechanism of Ca^{2+} induced Ca^{2+} release (CICR), whereby release of Ca^{2+} through one IP_3R channel will tend to promote the opening of neighboring channels. To appropriately control this potentially explosive regenerative process, IP_3Rs are distributed in a clustered manner across the ER surface (2). This results in a hierarchical organization of Ca^{2+} signals involving stochastic recruitment of varying numbers of IP_3Rs (4–6). Ca^{2+} release may be restricted to only a single channel, resulting in a tiny Ca^{2+} signal known as a blip; or opening of one channel may trigger other IP_3Rs within a cluster

†To whom correspondence should be addressed. ismith@uci.edu.

to generate a larger local Ca^{2+} signal known as a puff. Finally, higher levels of [IP_3] may evoke Ca^{2+} waves that propagate throughout the cell in a saltatory manner via recruitment of multiple puff sites by successive cycles of Ca^{2+} diffusion and CICR. The spatial localization of IP_3Rs is thus crucial for establishing and optimizing the spatio-temporal patterning of cytosolic Ca^{2+} signals that ensure appropriate regulation of downstream signaling pathways (7). However, important questions remain regarding how IP_3Rs aggregate into clusters and how this clustered organization is maintained.

Findings in *Xenopus* oocytes and various mammalian cell lines indicate that numerous puffs arise over many minutes at fixed locations within the cell, suggesting that IP_3R clusters are relatively stable entities (8–11) On the other hand, imaging studies employing GFP-tagged or immunostained IP_3Rs indicate that IP_3Rs can diffuse within the ER membrane (12–20), and that in resting cells they display a reticular pattern resembling that of other ER-localized proteins (11–14,16–21), suggesting that they are freely distributed throughout the ER. On the other hand, several publications describe the aggregation of IP_3Rs into clusters following sustained activation of IP_3 signaling and/or cytosolic [Ca^{2+}] elevation (12,17–20). In particular, recent reports (22,23) using patch-clamp recordings of excised nuclei from DT40 cells stably expressing type 1 or type 3 IP_3Rs demonstrated that IP_3Rs are freely diffusible within the lipid membrane, and that they rapidly (within a few seconds) cluster together when [IP_3] rises, resulting in a reduction of mean channel open probability and duration via postulated protein-protein interaction. Based on these findings, the authors hypothesize that dynamic regulation of the assembly and behavior of Ca^{2+} puff sites by IP_3 may play a physiological role in intact cells (22).

Here, we test this hypothesis of rapid and dynamic IP_3R clustering by utilizing total internal reflection (TIRF) fluorescence microscopy to resolve Ca^{2+} transients arising from openings of *individual* IP_3R channels in intact mammalian cells (24). We find that puffs arising as soon as 100–200 ms following photorelease of IP_3 involve no fewer IP_3R channels than do puffs occurring several seconds later. Moreover, sites where only a single IP_3R is active remain at fixed locations. We thus conclude that puff sites represent pre-established, stable clusters of IP_3Rs, and that functional IP_3Rs are not readily diffusible within the ER membrane.

RESULTS

Imaging puff and blip sites using TIRF microscopy

To examine whether IP_3Rs rapidly associate into clusters following stimulation by IP_3, we began by determining the numbers of IP_3R channels contributing to puffs evoked at different times following a step increase in [IP_3]. We loaded SH-SY5Y neuroblastoma cells with the fluorescent Ca^{2+} indicator fluo-4, together with a photolabile caged precursor (ci-IP_3) of the slowly-metabolized IP_3 analog iIP_3 and with the Ca^{2+} buffer EGTA by incubation with membrane-permeant esters of these compounds. We then used total internal reflection fluorescence (TIRF) microscopy to image local Ca^{2+} events evoked by delivering brief flashes of UV light to photorelease i-IP_3. As a result of the extremely thin (ca 100 nm) optical section of TIRF microscopy, in conjunction with the use of the slow Ca^{2+} buffer EGTA to suppress waves and 'sharpen' local Ca^{2+} gradients (25), fluo-4 fluorescence signals then closely reflect instantaneous Ca^{2+} flux from the ER, and it becomes possible to resolve Ca^{2+} flux through single IP_3Rs (9).

Cells were essentially quiescent before photorelease of ci-IP_3, while puffs were elicited shortly after a photolysis flash, and subsequently continued for tens of seconds (Fig.1A) (9). The latency after which puffs were first observed shortens with increasing photorelease (26), and reduced to as little as one or two hundred ms following strong stimuli, as in Fig. 1A. Fig. 1B illustrates the distribution of Ca^{2+} release sites in a representative cell, where activity was

detected at a total of 18 sites following weaker photo-release of i-IP_3. Ca^{2+} signals varied greatly between sites, with several locations showing frequent, large amplitude puffs (e.g. sites 3, 8, 9, 16), whereas others (e.g. sites 14, 17) displayed only small, 'rectangular' fluorescence blips that likely reflect openings of a single IP_3R channel (24). When examined on an expanded timescale, fluorescence traces showed distinct stepwise transitions during the falling phase of puffs, with dwell-state levels at approximate multiples of the unitary fluorescence level during blips (Fig. 2A). We had previously interpreted this quantal distribution of step amplitudes as arising from the differing numbers of IP_3R channels open at different times (24). Thus, it is possible to estimate the number of channels simultaneously open at the peak of a puff either by directly counting the numbers of discrete downward steps on the falling phase, or by taking the ratio of the peak fluorescence amplitude divided by the unitary channel amplitude ($\Delta F/F_0$ 0.1±0.01 n=8 sites) corresponding to blip events.

Puff amplitudes do not increase with time after photorelease of IP_3

We argue that the amplitudes of sequential puffs evoked at a given site should increase progressively with time after a photolysis flash if individual IP_3Rs are initially distributed at random but subsequently aggregate into clusters over several seconds in response to the step increase in [IP_3]. Fig 2B plots the peak fluorescence amplitudes of puffs as a function of time from the beginning of the UV flash: measurements of the first puff observed at each site are indicated by filled symbols, and subsequent puffs by open symbols. These data were obtained using a relatively strong flash that evoked initial puffs with short latency (range 60–200 ms: mean 142 ± 10 ms, n=16 puff sites). The mean amplitude of these short-latency puffs was $\Delta F/F_0$ 0.44 ± 0.06, corresponding to the simultaneous opening of 4–5 IP_3R channels. Subsequent puffs occurring at the same sites after latencies of 0.5–5s were on average somewhat smaller ($\Delta F/F_0$ 0.26±0.03, n=30 corresponding to about 2–3 channels), and the overall trend showed a progressive decrease in amplitude with time after the flash (Fig. 2B). Thus, it appears that on average there are already four or five IP_3Rs clustered at a puff site within 200 ms or sooner following the onset of photorelease of iIP_3, and the observation that subsequent puffs were no larger in amplitude suggests that the number of IP_3Rs per cluster did not further increase at later times.

However, we were concerned to exclude the progressive decline in puff amplitude did not result from some other mechanism which may have overshadowed a progressive recruitment of IP_3Rs over several seconds. Degradation of photoreleased iIP_3 is unlikely to account for the diminution of the puffs, as this analogue is slowly metabolized, and puff amplitudes are relatively sustained following weak photorelease (9). Instead, the large and frequent Ca^{2+} events evoked by strong photorelease of i-IP_3 tended to overpower the ability of the exogenously loaded EGTA to effectively clamp basal Ca^{2+}, resulting in a progressive elevation of basal cytosolic [Ca^{2+}] that may have inhibited IP_3Rs to cause the diminished puff amplitude (9). We therefore repeated these experiments using a weaker UV flash (Fig. 2C), so that basal [Ca^{2+}] remained stable. As expected (26), the latencies to the first puff at each site became appreciably longer (range 200–4000 ms; mean 1.9 ± 0.5s, n=18). Nevertheless, concordant with results using the strong flash, puff amplitudes at shorter latencies were slightly greater than those at longer times (mean $\Delta F/F_0$ = 0.48 ±0.09, n=18 for puffs with latencies 200–800 ms *versus* $\Delta F/F_0$ = 0.42±0.05, n=27 for puffs with latencies 1–5 s. Moreover, we did not observe any preponderance of single-channel blip events preceding the onset of puffs, as might be expected if individual IP_3Rs were diffusing and aggregating into clusters during this time.

Our measurements with TIRF microscopy provide optimal resolution of puffs, but are necessarily restricted to those puff sites located adjacent to the plasma membrane and which lie within the evanescent field of the microscope. To then determine whether these superficial IP_3Rs may behave differently to ones located deeper in the cell we imaged SH-SY5Y cells by

wide-field epi-fluorescence microscopy, focused in the center of the cells 4–5 μm inward from the cover glass. After evoking puffs by a photolysis flash and recording for several seconds, we then rapidly switched to TIRF illumination to identify the locations of superficial puff sites so they could be excluded from analysis. Initial puffs at 'deep' sites again arose after short latencies (258 ± 45 ms, n = 20 puff sites). Mean puff amplitudes showed no increase between initial and subsequent puffs at the same sites (respective amplitudes for 1st, 2nd, and 3rd puffs; $\Delta F/F_0$ = 0.61 ± 11, 0.52 ± 12, and 0.49 ± 12). Thus, the behaviour of superficial puff sites imaged by TIRF microscopy appears representative of the population of sites throughout the cell.

Puffs in HeLa cells and astrocytes

SH-SY5Y neuroblastoma cells are reported to express predominantly the type I IP_3R (11,27), but may also contain relatively low levels of both the type 2 (11,28) and type 3 IP_3R (11,29). To then investigate whether other cell lines that express differing proportions of IP_3R subtypes may undergo dynamic clustering, we repeated similar imaging studies in HeLa cells, that are reported to express a mixture of both type 1 and 3 IP_3Rs (30), and in astrocytes, which express mainly type 2 IP_3Rs (31,32). TIRF imaging in both these mammalian cell types revealed step-wise changes in fluorescence reminiscent of puffs in SH-SY5Y cells (upper panels, Fig. 3A,B). In both cell types the mean puff amplitudes were smaller than in SH-SY5Y cells ($\Delta F/F_0$ 0.38 ±0.03, n=91 puffs in SH-SY5Y cells; 0.24±0.01, n=89, in HeLa cells; 0.18±0.01, n=91, in astrocytes). This reduction is attributable to the opening of fewer IP_3R channels, because the unitary blip amplitudes were similar among all three cell types ($\Delta F/F_0$ 0.1±0.01 n=8; 0.1±0.01 n=15; and 0.11±0.01 n=8 for SH-SY5Y, HeLa and astrocyte cells, respectively). Nevertheless, it was clear that puffs occurring within latencies of less than a few hundred milliseconds involved openings of multiple IP_3R channels, and that puff amplitudes showed no significant increase as a function of time following photorelease of iIP_3 in either HeLa cells or astrocytes (lower panels, Fig. 3A,B).

Lack of motility of single IP_3Rs

To further test the hypothesis that individual IP_3Rs are motile and may diffuse and aggregate into clusters following IP_3 stimulation, we examined the behavior of sites that showed repetitive single-channel activity (blips) following photorelease of iIP_3 (Fig. 4A). We located the position of channels with high precision by fitting a 2-dimensional Gaussian function to fluorescence images of blips for every frame during which the channel was open, and then calculated the mean location over successive frames during individual openings. The image in Fig. 4B shows an SH-SY5Y cell with circles marking all sites where puffs (multi-channel Ca^{2+} signals) were observed, and the small rectangle marks the region around a blip site from which the fluorescence trace in Fig. 4A was obtained. This region is shown on an enlarged scale on the right, plotting the mean and standard error of centroid locations of the fluorescence signals during each of the 10 channel openings evident in the fluorescence trace. The position of the channel deviated by no more than 300 nm during ten seconds after the flash - a negligible movement as compared to the distance of about 5 μm to the nearest neighboring puff sites. The channel illustrated in Fig. 4A showed unusually long openings, possibly reflecting modal gating behavior of the IP_3R (33), which enhanced the precision of localization. However, a similarly restricted motility was observed for other sites that displayed only brief blips (e.g. site 17 in Fig. 1B). Analysis of 15 blip sites indicated an upper bound of about 0.012 $\mu m^2 s^{-1}$ for the 2-dimensional diffusion coefficient of single IP_3Rs.

The lack of influence of IP_3 on the distribution of single IP_3Rs is further supported by an analysis of blip frequency following photo-release of IP_3. If IP_3 causes IP_3Rs to cluster together, we expect that sites that display exclusively single-channel activity would become less frequent with increasing time after photorelease of iIP_3. This was not the case. Fig 4C plots

the total numbers of blips observed within successive 2s time bins after the photolysis flash (n=15 blip sites in 14 cells), showing that the occurrence of blips did not diminish over the 16 s following photo-release of i-IP_3.

Modeling the diffusive aggregation of IP_3Rs

Is it possible that IP_3Rs could diffuse and aggregate into clusters within a mean time as short as 150ms following photorelease of IP_3? To address this question, we performed Monte Carlo simulations of diffusive movement of IP_3Rs across the surface of the cell illustrated in Fig. 1B. We approximated the outline of the cell as a rectangle with dimensions of 10 × 20 μm and initially distributed some number N of IP_3Rs at random throughout this area. The IP_3Rs were represented as circles of diameter 20 nm, and diffused with a 2-dimensional diffusion coefficient D. Given that puffs recur at fixed locations, we modelled cluster formation as the aggregation of IP_3Rs at defined 'anchor points' corresponding to the locations of 7 puff sites in the cell where multi-channel events were observed, instead of assuming that clusters arise from random association of IP_3Rs (22). The anchor points represented a fixed cytoskeletal structure with diameter L. Beginning from time $t = 0$ we assumed that [IP_3] was instantaneously elevated so that random collision of an IP_3R with an anchoring point resulted in irreversible binding, and recorded the increasing numbers of IP_3Rs bound at each puff site as a function of time.

Fig. 5A shows a simulation where the number N of functional IP_3Rs was set to 100, based on the cell of Fig. 1B by counting the numbers of simultaneously open channels during the largest puff at each site plus those channels at lone sites. Studies employing fluorescence recovery after photobleaching (FRAP) suggest that a majority of IP_3Rs are mobile, but published estimates of the diffusion coefficient vary widely from ~0.01 $\mu m^2 s^{-1}$ to 0.45 $\mu m^2 s^{-1}$ (12–16). Our own estimate (0.012 $\mu m^2 s^{-1}$) derived from tracking functional blip sites, falls at the lower end of this range. Initially, we took a middle value of D = 0.1 $\mu m^2 s^{-1}$, as assumed by Taufiq et al. (22), and assumed a diameter L = 20 nm for the puff anchoring sites. Our experimental data (Fig. 2B) indicate that following strong photorelease of IP_3 the first puffs at a given site on average involve simultaneous openings of 4–5 IP_3R channels, and arise after a mean latency of about 150 ms. In contrast, the simulation in Fig. 5A with the above parameter values predicts that about one minute would pass before puff sites had, on average, accumulated 4 IP_3Rs.

Figs. 5B–D show similar simulations changing one parameter value at a time, as indicated. In Fig. 5B the diameter of the anchoring site was increased to 300nm, which has been estimated as the cluster size over which IP_3Rs are distributed at puff sites in oocytes (34). This resulted in a modest acceleration of clustering rate, but nevertheless it took over 30 s for an average of four IP_3Rs to accumulate in a cluster. In Fig. 5C we increased the number N of IP_3Rs per cell by ten-fold to 1000, while keeping D = 0.1 $\mu m^2 s^{-1}$ and L = 20 nm. As expected the rate of clustering was greatly accelerated, such that sites had accumulated an average of about four IP_3Rs after about 4 seconds; but even in this case most puff sites had not yet accumulated even a single IP_3R after 200 ms (inset, Fig. 5C). Finally, we note that most published values of the diffusion coefficient for IP_3Rs are appreciably lower than 0.1 $\mu m^2 s^{-1}$ (12–14, 16), as is our estimate (<0.012 0.1 $\mu m^2 s^{-1}$) based on the motility of blip sites. In Fig. 5D we thus illustrate a simulation with D = 0.03 $\mu m^2 s^{-1}$, which predicts that it would take over a minute before puff sites contained an average of even two IP_3Rs.

Discussion

IP_3Rs are located within the membrane of the ER, which forms a contiguous reticulum extending throughout the cytoplasm. Several reports indicate that a large fraction of IP_3Rs are mobile within the ER membrane (12–20), and that they are distributed uniformly at rest so that

the pattern of GFP-tagged or immunostained IP_3Rs resembles that of the ER itself (11–14, 16–21). It is thus surprising that functional imaging studies reveal that the local Ca^{2+} puffs that arise from clusters of IP_3Rs remain at fixed locations over many minutes (8–10). Although observations (12,17–20) that IP_3 itself induces the reversible aggregation of IP_3Rs into clusters could provide a resolution to this paradox, that explanation has never appeared attractive given that the clustering has been described as occurring over tens of seconds, whereas puff sites were evident within a few seconds following photorelease of IP_3 (24,35). In particular, we were prompted to further examine the kinetics of establishment and stability of puff sites by a recent report (22) indicating that IP_3Rs in the nuclear membrane aggregate in response to elevated $[IP_3]$ in as short a time as 2 s, and undergo a resulting change in channel gating properties. On the basis of those results, the authors proposed that dynamic regulation of clustering by IP_3 facilitates hierarchical recruitment of the elementary events that underlie all IP_3-evoked Ca^{2+} signals (22,23).

We employed a TIRF imaging technique capable of resolving the contributions of individual IP_3R channels to show that puffs involving several closely adjacent channels can already be evoked within 100–200 ms of IP_3 stimulation in mammalian cell types with differing expression profiles of IP_3R subtypes. In contrast, our simulations (Fig. 5) indicate that, based on reasonable assumptions for their density and diffusion coefficient, it would take many seconds or minutes for sufficient IP_3R channels to diffuse and aggregate into clusters. It is thus improbable that the large amplitude, multi-channel puffs we observe within a few hundred milliseconds after photorelease of IP_3 could arise because IP_3Rs undergoing random walk motility redistribute under the influence of IP_3 into clusters by a diffusional trap mechanism. Moreover, we find other discrepancies with the proposal of dynamic IP_3-dependent regulation of puff sites. Taufiq et al. (22) report that clustering results in a down-regulation of IP_3R function and reduction of channel mean open probability, so that a flurry of single-channel activity would be expected before IP_3Rs had time to associate into clusters. We did not observe this, even following weak photorelease of IP_3 where the clustering time may be slowed. Also, we demonstrate that successive puffs at a given site do not grow in amplitude, as predicted for progressive recruitment of IP_3Rs, and that 'lone' functional IP_3Rs display very limited motility. Taken together, these observations fail to support a physiological role for IP_3 in dynamically regulating IP_3R localization at puff sites in intact cells.

Is it possible, however, that clustering is still induced by IP_3, but that resting levels of IP_3 in the cell are already high enough to cause constitutive aggregation of IP_3R into clusters preformed before the photolysis flash? This appears unlikely because Ca^{2+} activity was almost nonexistent prior to photorelease of iIP_3. Although we cannot exclude that some basal level of $[IP_3]$ is present, it would be surprising if this were sufficient to regulate IP_3R clustering and yet fail to induce any appreciable Ca^{2+} liberation. Moreover, even if a low basal $[IP_3]$ could be responsible for constitutive clustering of IP_3Rs, this would it render moot the notion of a *dynamic* rearrangement of IP_3R signalling architecture in response to stimulation.

How then might our data be reconciled with several studies suggesting that a substantial population of IP_3Rs are freely diffusible within the ER membrane (12–20), and undergo a global reorganisation following stimulation? (12,17–20,36). One possibility is that our stimuli did not elevate cytosolic $[IP_3]$ sufficiently to effect IP_3R clustering. However, this seems unlikely because, although cells were loaded with the slow Ca^{2+} buffer EGTA to deliberately inhibit cluster-cluster interactions and suppress global Ca^{2+} waves, photolysis flash strengths equivalent or weaker than those used here produce robust and long lasting (minutes) global increases in cytosolic free $[Ca^{2+}]$ in the absence of EGTA (9).

A more likely explanation lies in the difference that we monitored those IP_3Rs that show functional Ca^{2+} release under physiological conditions, whereas most previous studies

localized IP_3R proteins either by tagging exogenously expressed receptors with fluorescent proteins (12–19) and/or by immunostaining of endogenous IP_3Rs (11,17,20). As noted above, both of these approaches show IP_3Rs as being expressed throughout the the ER (For examples see Fig. 1 of (18); Fig. 1 of (12), and Fig. 2 of (20)). On this basis one would expect that IP_3-evoked Ca^{2+} release would be apparent throughout the entirety of the cell cytoplasm, yet numerous reports have shown that this is clearly not the case. Instead, Ca^{2+} release in various mammalian cells arises at just a few discrete puff sites (9–11,24,37,38), and puff sites appear to be anchored in place as they do not move even in the face of sustained elevations of IP_3 that evoke repetitive Ca^{2+} waves (39). We thus propose that cells may contain two different populations of IP_3Rs: (i) A subset that are anchored together in pre-formed clusters by association with static cytoskeletal structures and which, possibly as a consequence of this anchoring, display high sensitivity to IP_3 to generate Ca^{2+} puffs. (ii) A population of motile IP_3Rs that are either functionally unresponsive, or mediate Ca^{2+} liberation only during sustained global elevations of cytosolic [Ca^{2+}]. Interestingly, this scheme involves modulation of IP_3R function based upon their localization, but in the opposite sense to that proposed by Tafiq et al (22). That is to say, clustered IP_3R are preferentially activated under conditions that evoke puffs, rather than displaying a reduced open channel probability.

Cellular Ca^{2+} signalling is a highly regulated process, with localized increases in [Ca^{2+}] playing widely divergent physiological and pathophysiological roles depending on where in the cytosol these localized signals arise (1). We provide evidence that the sites generating local Ca^{2+} puffs represent pre-established, stable clusters of IP_3Rs; and further suggest that puff sites may be defined by the functional modulation and immobilization of IP_3Rs from a larger pool of diffusionally motile receptors when they bind to static cytoskeletal elements.

METHODS

Cell Culture

Human neuroblastoma SH-SY5Y cells were cultured as previously described (9) in a mixture (1:1) of Ham's F12 medium and Eagle's minimal essential medium, supplemented with 10% (v/v) fetal bovine serum (FBS) and 1% nonessential amino acids. Cells were incubated at 37 °C in a humidified incubator gassed with 95% air and 5% CO_2, passaged every 7 days and used for up to 20 passages. A few days prior to imaging, cells were harvested in phosphate-buffered saline (PBS) without Ca^{2+} or Mg^{2+} and sub-cultured in Petri dishes with glass coverslips as the base (MatTek) at a seeding density of 3×10^4 cells/ml. HeLa cells were cultured in a similar manner except that the culture media consisted of DMEM supplemented with 10% FBS and 1% Pen/Strep.

To obtain astrocytes, cerebral cortices were removed from four 1–3 day old Sprague-Dawley rat pups and placed immediately in ice-cold buffer solution consisting of 10 mM NaH_2PO_4, 2.7 mM KCl, 137 mM NaCl, 14 mM glucose, 1.5 mM $MgSO_4$, and 3 mg/ml bovine serum albumin. Meninges were removed using fine forceps, whole cortices were then minced using fine forceps and placed into 0.125% trypsin-EDTA for 10 min. Trypsin digestion was halted by the addition of an equal volume of fresh astrocyte culture media (DMEM supplemented with 10% FBS and 1% Pen/Strep). The tissue was then pelleted by centrifugation at 4500 rpm for 5 min following which the supernatant was removed and the cell pellet resuspended in 2 ml of fresh media. The tissue was subsequently triturated gently with three fire-polished Pasteur pipettes of narrowing bore size. After allowing larger pieces of tissue to settle for 5 minutes, the supernatant was applied to a 40 μm cell strainer and 40 ml of fresh media was applied. This cell suspension was then aliquoted into 1 × 25cm^2 flasks and onto Petri dishes with glass coverslips as the base (MatTek). Cells were then kept in a humidified incubator at 37 °C (95% air; 5% CO_2). This was designated passage 1 and cells were used up to a passage of 2. Four to six hours following plating, cells were washed vigorously several times with fresh media to remove non-adhered

cells. This resulted in a culture of primarily type I cortical astrocytes (as confirmed by positive immunostaining with an anti-GFAP antibody). Culture medium was exchanged every 3–4 days and cells were grown in culture for up to 14 days. All recordings were made from cells between days 5–12.

Loading of cell permeant esters

Cells were loaded a few hours before use by incubation with HEPES-buffered saline (HBS: in mM; NaCl 135, KCl 5, $MgSO_4$ 1.2, $CaCl_2$ 2.5, HEPES 5, glucose 10) containing 1 μM ci-IP_3/PM (SiChem, Bremen, Germany) at room temperature for 45 mins, followed by incubation with 1 μM caged ci-IP_3/PM plus 5 μM fluo-4AM (Invitrogen, Carlsbad, CA) at room temperature for 45 min, and finally 1 hr with 5 μM EGTA-AM (Invitrogen, Carlsbad, CA).

Total Internal Reflection Microscopy

Imaging of changes in $[Ca^{2+}]_i$ was accomplished using a custom-built TIRF microscope system based around an Olympus IX 70 microscope equipped with an Olympus X60 TIRFM objective (NA 1.45). Fluorescence of cytosolic fluo-4 was excited within the ~100 nm evanescent field formed by total internal reflection of a 488 nm laser beam incident through the microscope objective at the coverglass/aqueous interface. Images of emitted fluorescence (λ >510 nm) were captured at a resolution of 128 × 128 pixels (1 pixel = 0.25 μm) at a rate of 420 frames s^{-1} by a Cascade 128 electron multiplied CCD camera (Roper Scientific). Photorelease of i-IP_3 from a caged precursor was evoked by flashes of UV (350–400nm) light derived from a fiber-optic arc lamp source introduced via a UV reflecting dichroic mirror in the upper side-port of the microscope. The UV light was adjusted to uniformly irradiate a region slightly larger than the imaging frame, and any given imaging field was exposed to only a single flash.

Image Processing and Analysis

Image processing and analysis were done using MetaMorph 7.5 (Molecular Dynamics). After subtraction of the camera black offset level, image sequences were first processed by dividing each frame by an average of ~100 frames captured before the photolysis flash, so that fluorescence represents a ratio ($\Delta F/F_0$) of the fluorescence change (ΔF) at each pixel relative to the mean resting fluorescence (F_0) prior to stimulation. The resulting image stack was then further processed by frame-by-frame subtraction of heavily smoothed (16 ×16 pixel low-pass filter) images, so as to correct for slow drift in basal fluorescence and fluctuations in laser power (40). Fluorescence traces like those in Fig. 1 were derived by measuring the average signal within 1 × 1 μm (3×3 pixel) regions of interest centered on visually-identified Ca^{2+} release sites. Puff latencies are expressed as the time from onset of the photolysis flash to onset of the puff. Single channel Ca^{2+}-fluorescence signals were localized by fitting to a circularly-symmetrical Gaussian function with a precision of 0.2 pixels, using a custom particle-tracking routine in Slidebook (Intelligent Imaging Innovations, Santa Monica, CA.). The amplitude was allowed to vary to achieve the best fit whereas the standard deviation was preset to 3 pixels (1.2 μm). Diffusion coefficients D were calculated from a regression fit to data plotting displacements of puff centroids as a function of time as $D = d2/4t$, where d = mean distance of the blip fluorescence during each opening from its origin at time t.

Stochastic simulation of IP_3R diffusion and clustering

The ER membrane within the plane of the TIRF image was simulated as a 2-dimensional rectangular domain with a size of 10 × 20 μm. A certain number N of IP_3R channels with diameter 20 nm were randomly distributed on the ER membrane at time $t = 0$ and underwent a random walk in both x and y directions by incrementing their positions at time-steps $\Delta t = 10$ μs by adding random numbers distributed as a Gaussian function centered around zero. The width (standard deviation) of the Gaussian was adjusted to achieve the desired macroscopic

diffusion coefficients. IP_3Rs hitting the boundaries were reflected back. For simplicity, we ignored collisions among IP_3Rs; that is to say, IP_3Rs passed through each other without deflection. Specific fixed sites were designated as IP_3R channel trap locations, based on the mapping in Fig. 1B. Each trap location was assumed to have a diameter L. An IP_3R channel moving within a distance of $L/2 + 10$ nm became fixed at that cluster site. For simplicity, we assumed that trapped channels did not affect the trap diameter or location. Fig. 5 shows the results of representative single simulations, counting the numbers of IP_3Rs trapped at each site as a function of time t, together with mean numbers of IP_3R per cluster derived from 50 simulations.

REFERENCES AND NOTES

1. Berridge MJ, Lipp P, Bootman MD. The versatility and universality of calcium signalling. Nat Rev Mol Cell Biol 2000;1:11. [PubMed: 11413485]
2. Foskett JK, White C, Cheung KH, Mak DO. Inositol trisphosphate receptor calcium release channels. Physiol Rev 2007;87:593. [PubMed: 17429043]
3. Bezprozvanny I, Watras J, Ehrlich BE. Bell-shaped calcium-response curves of inositol trisphosphate and calcium-gated channels from endoplasmic reticulum of cerebellum. Nature 1991;351:751. [PubMed: 1648178]
4. Lipp P, Niggli E. A hierarchical concept of cellular and subcellular calcium signalling. Prog Biophys Mol Biol 1996;65:265. [PubMed: 9062435]
5. Parker I, Choi J, Yao Y. Elementary events of I inositol trisphosphate-induced calcium liberation in Xenopus oocytes: hot spots, puffs and blips. Cell Calcium 1996;20:105. [PubMed: 8889202]
6. Yao Y, Choi J, Parker I. Quantal puffs of intracellular calcium evoked by inositol trisphosphate in Xenopus oocytes. J Physiol 1995;482:533. [PubMed: 7738847]
7. Shuai JW, Jung P. Optimal ion channel clustering for intracellular calcium signaling. Proc Natl Acad Sci U S A 2003;100:506. [PubMed: 12518049]
8. Dargan SL, Parker I. Buffer kinetics shape the spatiotemporal patterns of inositol trisphosphate-evoked calcium signals. J Physiol 2003;553:775. [PubMed: 14555715]
9. Smith IF, Wiltgen SM, Parker I. Localization of puff sites adjacent to the plasma membrane: Functional and spatial characterization of calcium signaling in SH-SY5Y cells utilizing membrane-permeant caged inositol trisphosphate. Cell Calcium 2009;45:65. [PubMed: 18639334]
10. Thomas D, Lipp P, Berridge MJ, Bootman MD. Hormone-evoked elementary calcium signals are not stereotypic, but reflect activation of different size channel clusters and variable recruitment of channels within a cluster. J Biol Chem 1998;273:27130. [PubMed: 9765231]
11. Tovey SC, et al. Calcium puffs are generic inositol trisphosphate-activated elementary calcium signals and are downregulated by prolonged hormonal stimulation to inhibit cellular calcium responses. J Cell Sci 2001;114:3979. [PubMed: 11739630]
12. Chalmers M, Schell MJ, Thorn P. Agonist-evoked inositol trisphosphate receptor clustering is not dependent on changes in the structure of the endoplasmic reticulum. Biochem J 2006;394:57. [PubMed: 16274363]
13. Cruttwell C, et al. Dynamics of the inositol trisphosphate receptor during polarization of MDCK cells. Biol Cell 2005;97:699. [PubMed: 15730344]
14. Ferreri-Jacobia M, Mak DO, Foskett JK. Translational mobility of the type 3 inositol trisphosphate receptor calcium release channel in endoplasmic reticulum membrane. J Biol Chem 2005;280:3824. [PubMed: 15537642]
15. Fukatsu K, et al. Lateral diffusion of inositol trisphosphate receptor type 1 is regulated by actin filaments and 4.1N in neuronal dendrites. J Biol Chem 2004;279:48976. [PubMed: 15364918]
16. Gibson CJ, Ehrlich BE. Inositol 1,4,5-trisphosphate receptor movement is restricted by addition of elevated levels of O-linked sugar. Cell Calcium 2008;43:228. [PubMed: 17610951]
17. Iwai M, et al. Molecular cloning of mouse type 2 and type 3 inositol trisphosphate receptors and identification of a novel type 2 receptor splice variant. J Biol Chem 2005;280:10305. [PubMed: 15632133]

18. Tateishi Y, et al. Cluster formation of inositol trisphosphate receptor requires its transition to open state. J Biol Chem 2005;280:6816. [PubMed: 15583010]
19. Tojyo Y, Morita T, Nezu A, Tanimura A. The clustering of inositol trisphosphate receptors is triggered by inositol trisphosphate binding and facilitated by depletion of the calcium store. J Pharmacol Sci 2008;107:138. [PubMed: 18544901]
20. Wilson BS, et al. Calcium-dependent clustering of inositol trisphosphate receptors. Mol Biol Cell 1998;9:1465. [PubMed: 9614187]
21. Kume S, et al. The Xenopus inositol trisphosphate receptor: structure, function, and localization in oocytes and eggs. Cell 1993;73:555. [PubMed: 8387895]
22. Taufiq Ur R, Skupin A, Falcke M, Taylor CW. Clustering of inositol trisphosphate receptors by inositol trisphosphate retunes their regulation by inositol trisphosphate and calcium. Nature 2009;458:655. [PubMed: 19348050]
23. Rahman T, Taylor CW. Dynamic regulation of inositol trisphosphate receptor clustering and activity by inositol trisphosphate. Channels (Austin) 2009;3:1. [PubMed: 19221508]
24. Smith IF, Parker I. Imaging the quantal substructure of single inositol trisphosphate receptor channel activity during calcium puffs in intact mammalian cells. Proc Natl Acad Sci U S A 2009;106:6404. [PubMed: 19332787]
25. Shuai J, Parker I. Optical single-channel recording by imaging calcium flux through individual ion channels: theoretical considerations and limits to resolution. Cell Calcium 2005;37:283. [PubMed: 15755490]
26. Callamaras N, Marchant JS, Sun XP, Parker I. Activation and co-ordination of inositol trisphosphate-mediated elementary calcium events during global calcium signals in Xenopus oocytes. J Physiol 1998;509:81. [PubMed: 9547383]
27. Wojcikiewicz RJ. Type I, II, and III inositol trisphosphate receptors are unequally susceptible to down-regulation and are expressed in markedly different proportions in different cell types. J Biol Chem 1995;270:11678. [PubMed: 7744807]
28. Mackrill JJ, Challiss RA, O'Connell D A, Lai FA, Nahorski SR. Differential expression and regulation of ryanodine receptor and myo-inositol trisphosphate receptor calcium release channels in mammalian tissues and cell lines. Biochem J 1997;327:251. [PubMed: 9355760]
29. Van Acker K, et al. inositol trisphosphate-mediated calcium signals in human neuroblastoma SH-SY5Y cells with exogenous overexpression of type 3 inositol trisphosphate receptor. Cell Calcium 2002;32:71. [PubMed: 12161107]
30. Hattori M, et al. Distinct roles of inositol trisphosphate receptor types 1 and 3 in calcium signaling. J Biol Chem 2004;279:11967. [PubMed: 14707143]
31. Holtzclaw LA, Pandhit S, Bare DJ, Mignery GA, Russell JT. Astrocytes in adult rat brain express type 2 inositol trisphosphate receptors. Glia 2002;39:69. [PubMed: 12112377]
32. Petravicz J, Fiacco TA, McCarthy KD. Loss of inositol trisphosphate receptor-dependent calcium increases in hippocampal astrocytes does not affect baseline CA1 pyramidal neuron synaptic activity. J Neurosci 2008;28:4967. [PubMed: 18463250]
33. Ionescu L, et al. Mode switching is the major mechanism of ligand regulation of InsP3 receptor calcium release channels. J Gen Physiol 2007;130:631. [PubMed: 17998395]
34. Shuai J, Rose HJ, Parker I. The number and spatial distribution of inositol trisphosphate receptors underlying calcium puffs in Xenopus oocytes. Biophys J 2006;91:4033. [PubMed: 16980372]
35. Sun XP, Callamaras N, Marchant JS, Parker I. A continuum of inositol trisphosphate-mediated elementary calcium signalling events in Xenopus oocytes. J Physiol 1998;509:67. [PubMed: 9547382]
36. Dargan SL, Demuro A, Parker I. Imaging calcium signals in Xenopus oocytes. Methods Mol Biol 2006;322:103. [PubMed: 16739719]
37. Bootman M, Niggli E, Berridge M, Lipp P. Imaging the hierarchical calcium signalling system in HeLa cells. J Physiol 1997;499:307. [PubMed: 9080361]
38. Bootman MD, Berridge MJ, Lipp P. Cooking with calcium: the recipes for composing global signals from elementary events. Cell 1997;91:367. [PubMed: 9363945]
39. Marchant JS, Parker I. Role of elementary calcium puffs in generating repetitive calcium oscillations. Embo J 2001;20:65. [PubMed: 11226156]

40. Demuro A, Parker I. "Optical patch-clamping": single-channel recording by imaging calcium flux through individual muscle acetylcholine receptor channels. J Gen Physiol 2005;126:179. [PubMed: 16103278]

41. We thank Karl Kilborn (Intelligent Imaging Innovations) for writing the custom localization routine. This work was supported by grants GM 48071 and GM 65830 from the National Institutes of Health, and by a University of California Systemwide Biotechnology Research & Education Program GREAT Training Grant 2008-14 to S.W.

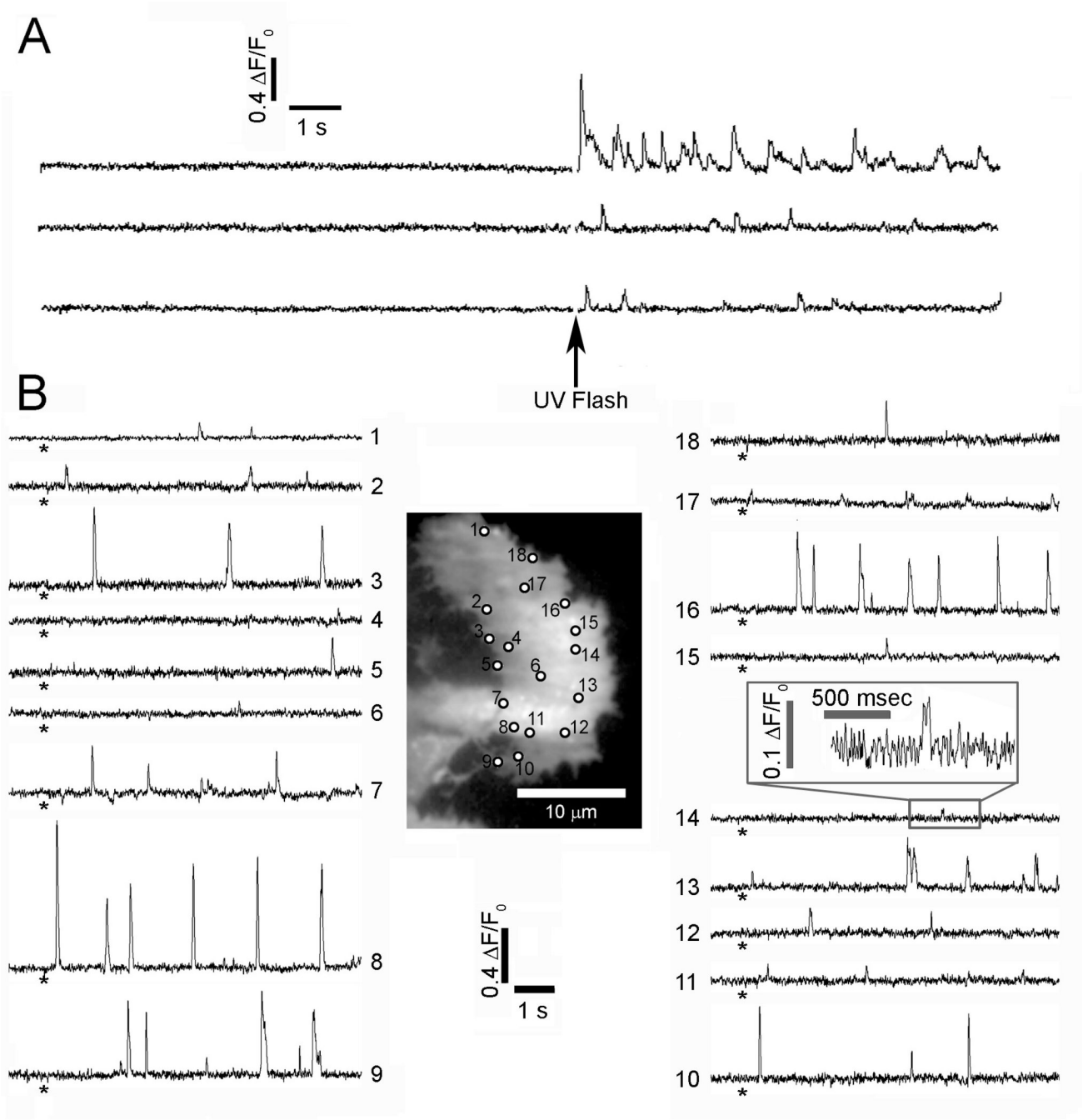

Fig. 1.

Local Ca^{2+} signals evoked in SH-SY5Y cells following photorelease of i-IP_3. (A) Representative fluorescence traces recorded from 3 puff sites monitored by TIRF microscopy. The records include long baseline sections before a strong (40 ms) photolysis flash (arrow), demonstrating a lack of basal spontaneous activity. Traces show fluorescence ratio changes ($\Delta F/F_0$) of fluo-4, monitored from 3 × 3 pixel (1 × 1 μm) regions of interest. (B) TIRF image shows resting fluorescence of a single fluo-4-loaded SH-SY5Y cell. Circles mark all sites where Ca^{2+} signals were evident following photorelease of i-IP_3. Traces show fluorescence ratio signals ($\Delta F/F_0$) measured from each of the numbered sites marked on the cell image.

Asterisks indicate the time of a weak (35 ms) photolysis flash. The inset box shows a single blip at site #14 on enlarged scales.

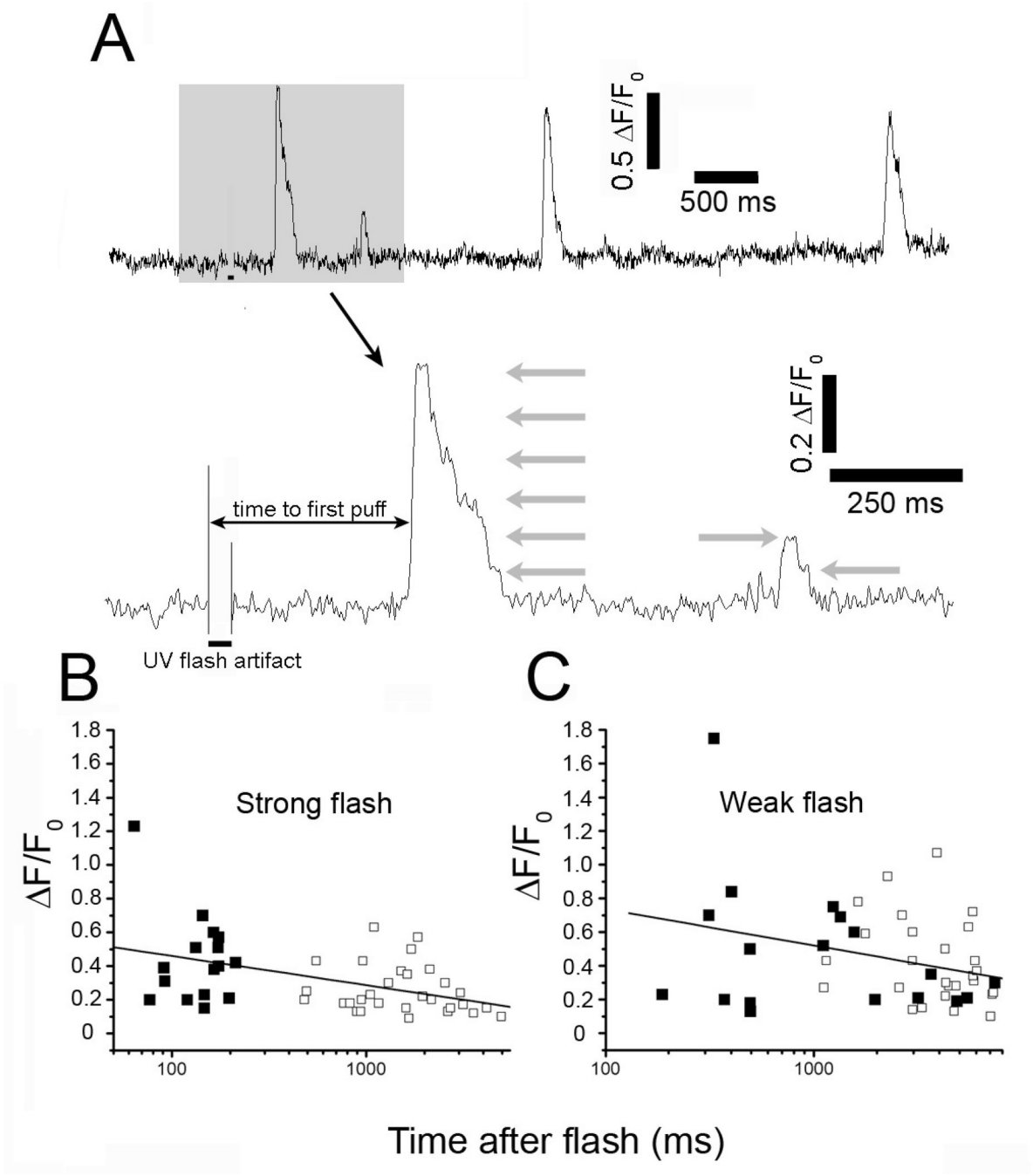

Fig. 2.

Puffs evoked at short latencies following photorelease of i-IP_3 involve similar or greater numbers of IP_3R channels than puffs at longer latencies. (A) Representative fluorescence trace ($\Delta F/F_0$) depicting the first 4 events evoked at a single site following a UV flash. Lower trace shows the first two events (highlighted grey) shown on an expanded time scale showing stepwise transitions in Ca^{2+} fluorescence at approximate multiples of the unitary event level (grey arrows). Solid bars underneath each trace indicate the duration of the UV flashes. (B, C), Plots show peak puff amplitudes as a function of time after onset of the photolysis flash for strong and weak photolysis strengths, respectively. Filled squares denote the amplitude of the

first event at each site, with subsequent events at those sites shown as hollow squares. Lines are regression fits to data on semi-logarithmic axes.

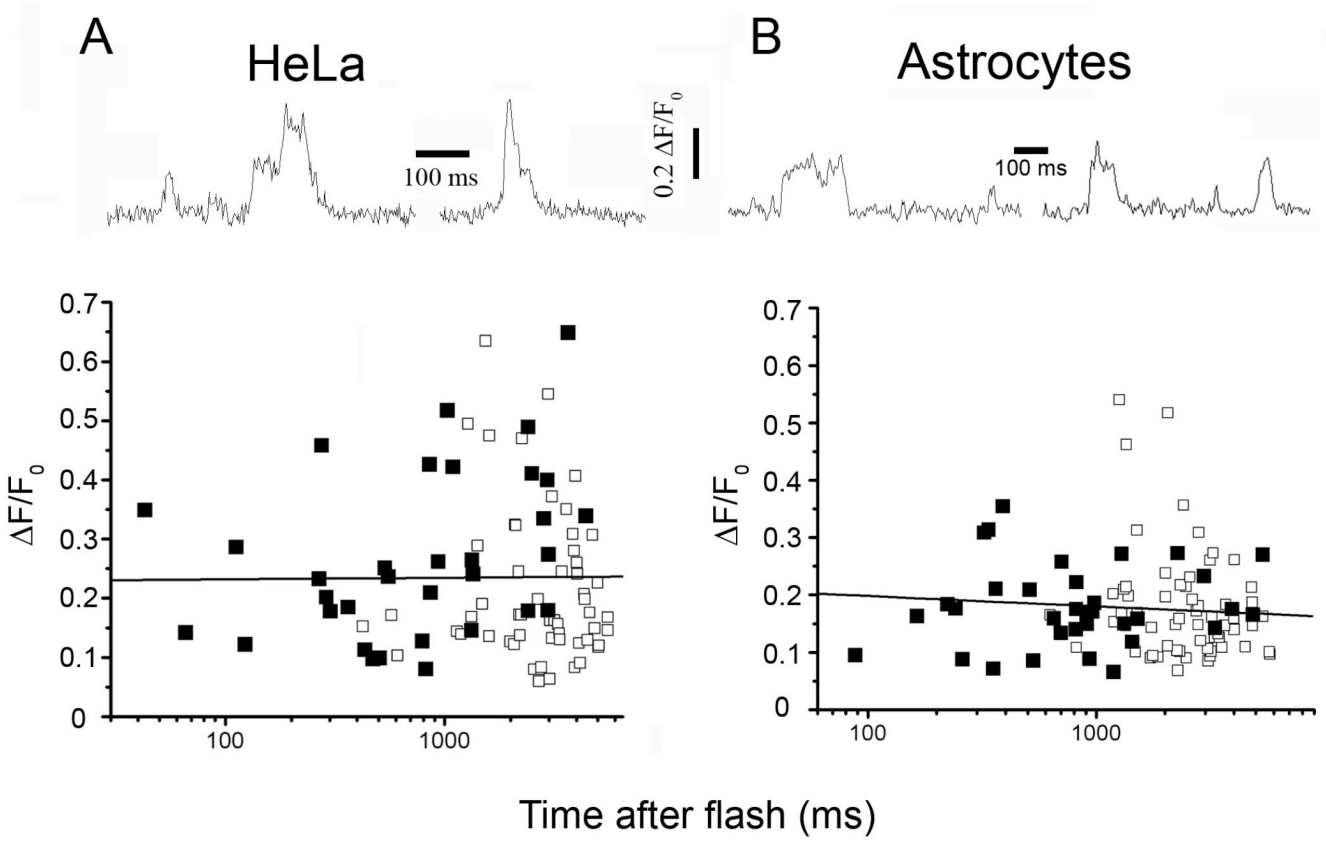

Fig. 3.

Ca^{2+} signals evoked by photorelease of i-IP_3 in HeLa (A) and rat type I cortical astrocytes (B), recorded with single-channel resolution. The traces at the top show representative events displaying step-wise transitions in Ca^{2+} fluorescence. Signals in both of these cell types were on average smaller than in SH-SY5Y cells, and fewer step levels were evident. Plots show peak amplitudes of first (filled squares) and subsequent (open squares) events as functions of time after a strong (40 ms) photolysis flash. Lines are regressions to data on semi-logarithmic axes.

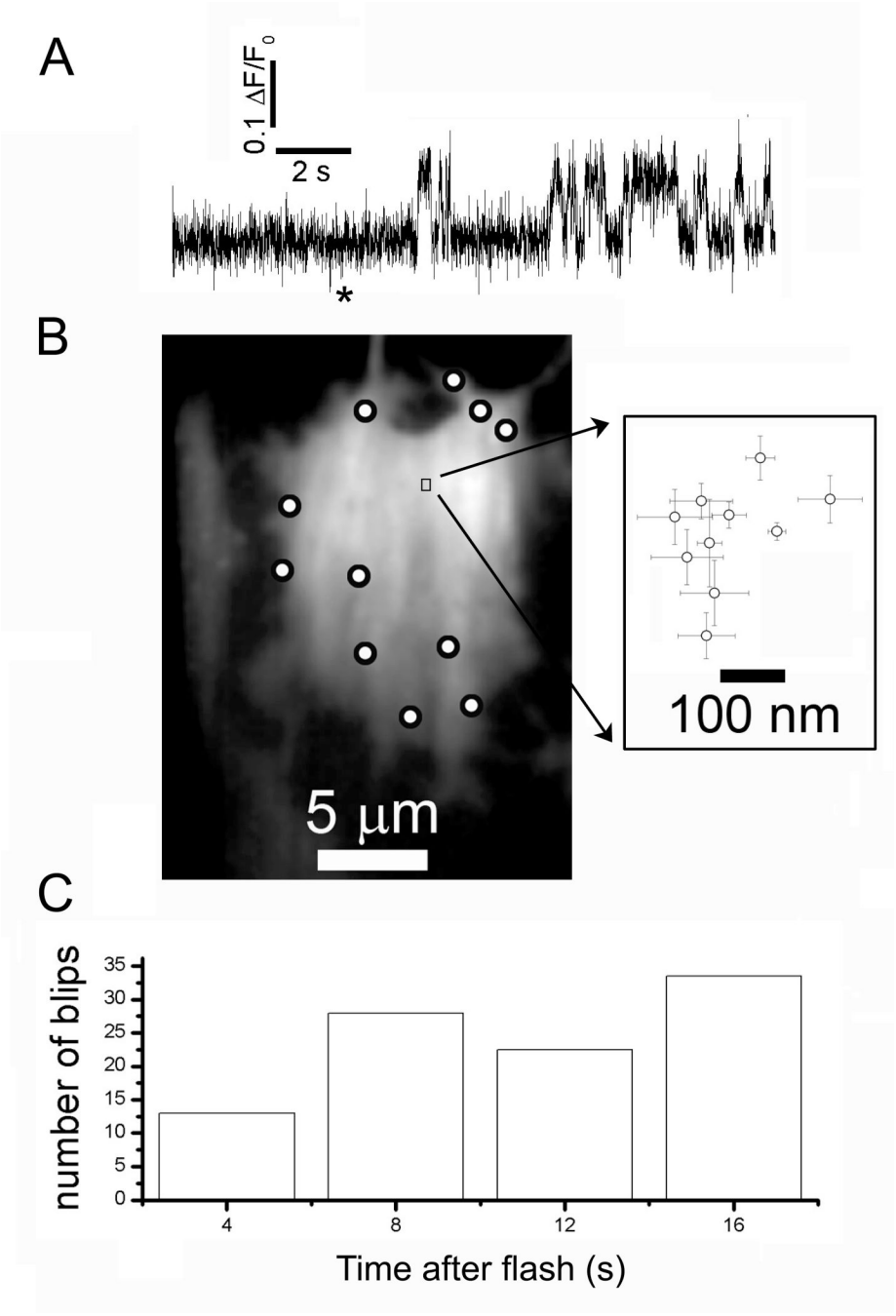

Fig. 4.

Lack of motility of single IP_3Rs. (A) Representative trace showing activity from an apparent 'lone' IP_3R following a (200 ms) photolysis flash (asterisk). Fluorescence was measured from a 1 μm square region of interest. (B), The image shows resting fluorescence of a single fluo-4-loaded SH-SY5Y cell, with the locations of all sites showing puffs (multi-channel signals) marked by circles, and with the site from which the trace in A was obtained marked by the box. The inset shows a scatter plot of mean centroid positions (error bars = ± 1SEM) of Ca^{2+} fluorescence during each of the discrete openings (blips) in the trace in A. (C) Bar graph shows the numbers of blips occurring during successive 2s intervals following photorelease of i-IP_3, derived from 15 sites that displayed exclusively single channel activity.

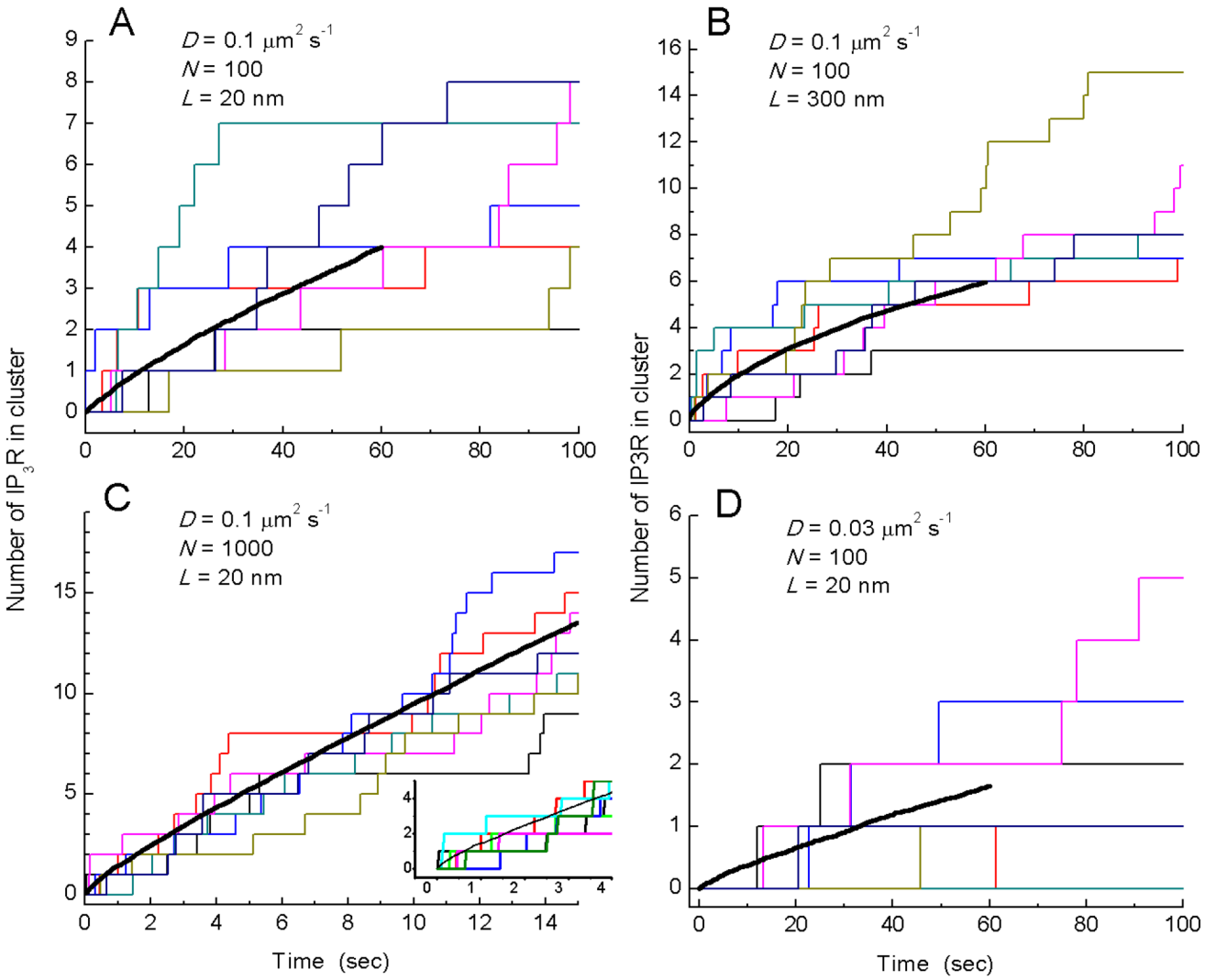

Fig. 5.

Modeling cluster formation by a diffusive trap mechanism. Graphs show the numbers of IP_3Rs clustered at each of 7 puff sites in a simulated cell (colored step-wise lines), and the mean number of IP_3Rs per cluster (black curves; average of 50 simulations, 350 puff sites) as functions of time. The simulations model diffusion within a 2-dimensional rectangular cell (10 × 20 μm) in which *N* IP_3Rs are initially distributed at random and subsequently diffuse with diffusion coefficient *D*. Seven 'anchoring' sites with diameter *L* represent puff sites, to which IP_3Rs adhere after colliding. Panels show simulations with the following respective values of *D* ($\mu m^2\ s^{-1}$), *N* and *L* (nm) : (A) 0.1, 100, 20; (B) 0,1, 100, 300; (C) 0.1, 1000, 20; (D) 0.03, 100, 20.